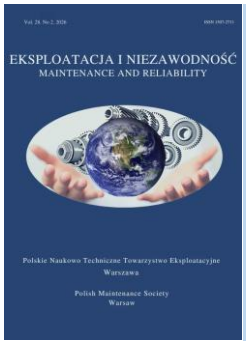

Eksploatacja i Niezawodnosc – Maintenance and Reliability
Volume 28 (2026), Issue 2
journal homepage: http://www.ein.org.pl

Article citation info:
Yetgin A, Experimental Analysis of the Effects of Rotor End Ring Fin Failure on Thermal, Vibration and Performance of Three-Phase Squirrel Cage Induction Motor, Eksploatacja i Niezawodnosc – Maintenance and Reliability 2026: 28(2) http:/10.17531/ein/210684

Experimental Analysis of the Effects of Rotor End Ring Fin Failure on Thermal, Vibration and Performance of Three-Phase Squirrel Cage Induction Motor

Indexed by:

Asım Gökhan Yetgin[a,*]

[a] Faculty of Engineering And Architecture, Dept. of Elec. Elt. Eng., Burdur Mehmet Akif Ersoy University, Turkey

Highlights

- The effect of rotor fins on motor temperature and vibration was analysed experimentally.
- If there was no cooling in the rotor, the motor performance was negatively affected.
- Failure in the rotor fins negatively affected motor balance and increased vibration.

Abstract

Induction motors have a robust structure. However, they may encounter internal and external failures. These faults can lead to deterioration of motor performance and even to the stopping of the process. In addition, various faults that may occur in the motor cause the motor temperature to increase and result in a reduction in the lifespan of the motor. The aim of this study is to investigate the faults occurring in the cooling fins in the rotor end ring of a three-phase squirrel cage induction motor and the effects of these faults on motor performance, motor vibration and motor temperature. No-load operation, short circuit operation and loaded operation tests were performed on the healthy motor and the motor with defective rotor fins, during which both vibration and thermal images were obtained from both motors. The results showed that the shaving of the rotor fins caused an extra vibration in the motor. The absence of rotor fins, which also served as cooling, caused the thermal temperatures of the motor to increase and the motor performance to deteriorate. Motor efficiency decreased by 1% as a result of changing the equivalent circuit parameters. Data obtained from the no-load and short-circuit tests showed that the temperature values of the faulty motor were 5% and 5.64% higher than those of the healthy motor, and in the loaded test, the temperature value of the faulty motor was 1.14% higher.

Keywords
induction motor, rotor cooling fin failure, performance analysis, thermal analysis, vibration analysis.

1. Introduction

Squirrel Cage Induction Motors (SCIMs) are widely used today in many applications such as pumps, compressors, conveyors, machine tools and other industrial devices [1]. Despite their robustness, reliability, low-cost [2] good work parameters [3], and ease of maintenance [4], induction motors are prone to failure due to exposure to various harsh environments and incorrect operating conditions or manufacturing defects [5]. Although these motors are extremely reliable and robust, they can fail prematurely due to unforeseen reasons such as environmental, thermal and mechanical stresses [6]. Induction Motors (IMs) are the most widely used electrical machines in industry. For this reason, a malfunction in the motor can cause both cost loss and disruption of the production process in the enterprise. Faults may occur in IMs due to reasons such as imbalance in voltage and current values, overloading, thermal effects, environmental effects, unhealthy working environment,

(*) Corresponding author.
E-mail addresses: A.G. Yetgin (ORCID:0000-0003-3971-0504) agyetgin@mehmetakif.edu.tr

faults during manufacturing, vibration, grounding fault, faults in windings, falling to single phase, etc. [7]. During operation, mechanical or electrical faults may occur in the stator or rotor of the motor or both at the same time [8]. The percentage changes in faults in IMs by IEEE (Institute of Electrical and Electronics Engineers) and EPRI (Electric Power Research Institute) are given in Figure 1 [9].

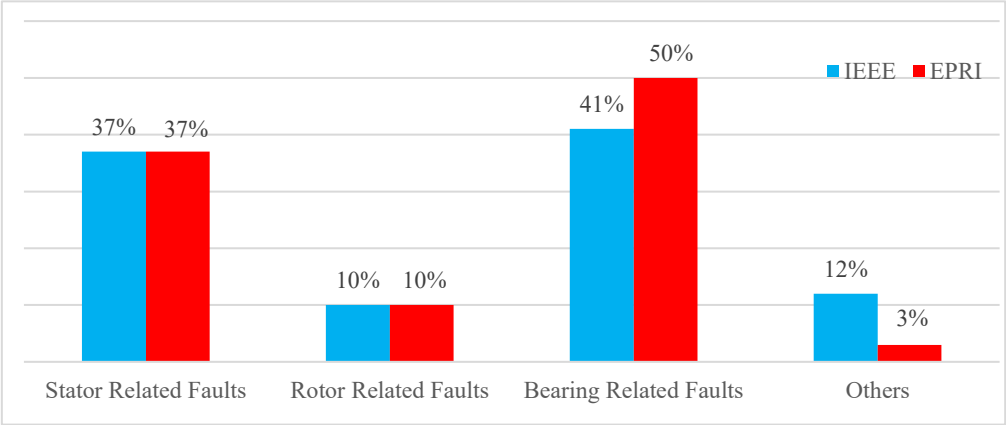

Figure 1. Percentage changes of induction motor failures.

Faults in IMs are generally classified as internal and external faults [10]. These faults are grouped into three subgroups: electrical, mechanical and environmental. The types of faults that can occur in an IM are given in Figure 2 [11].

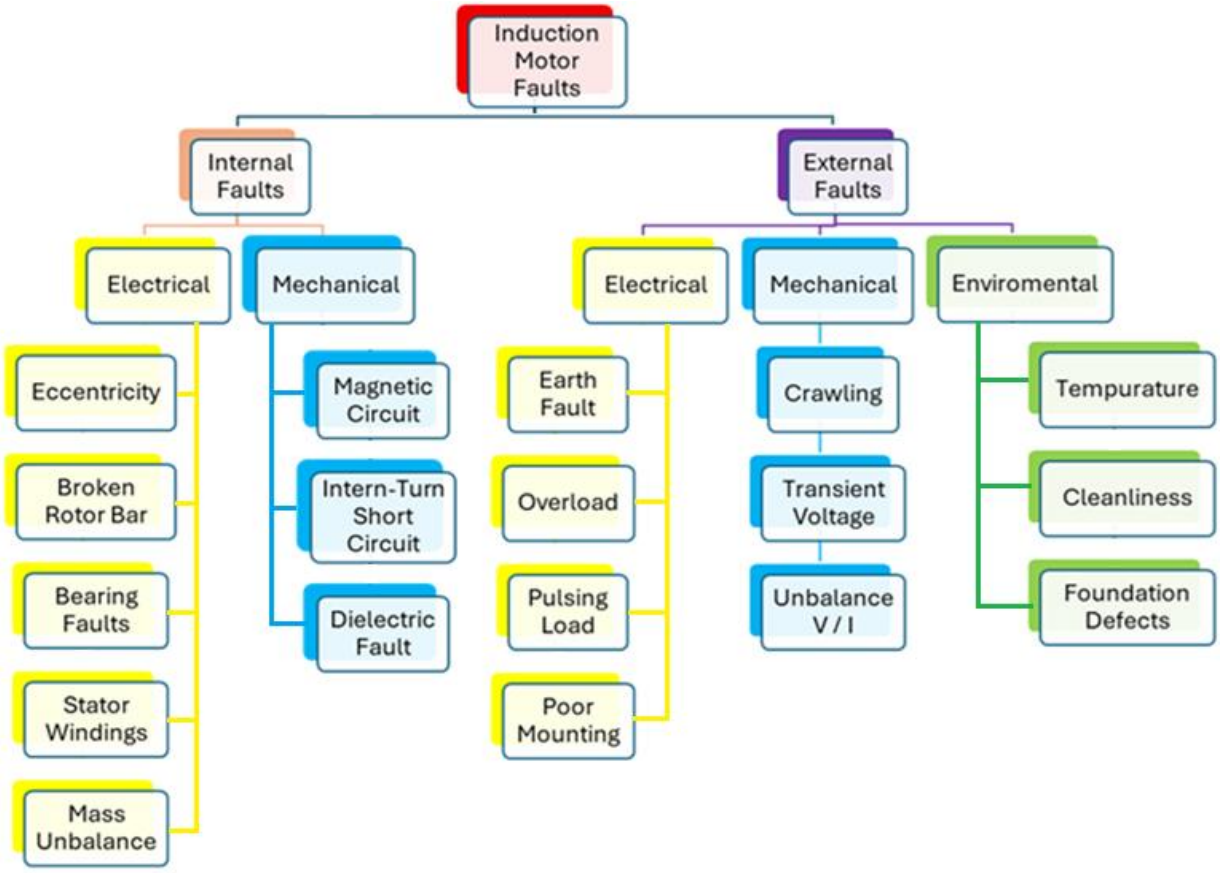

Figure 2. Induction motor fault types.

During the operation of the IM, losses due to heat (core losses, stator copper losses and rotor losses) affect the efficiency and performance of the motor, and these losses cause some important problems when the temperature reaches values greater than the allowable operating temperature [12]. The effects of increasing temperature on the IMs are given in Figure 3 [13].

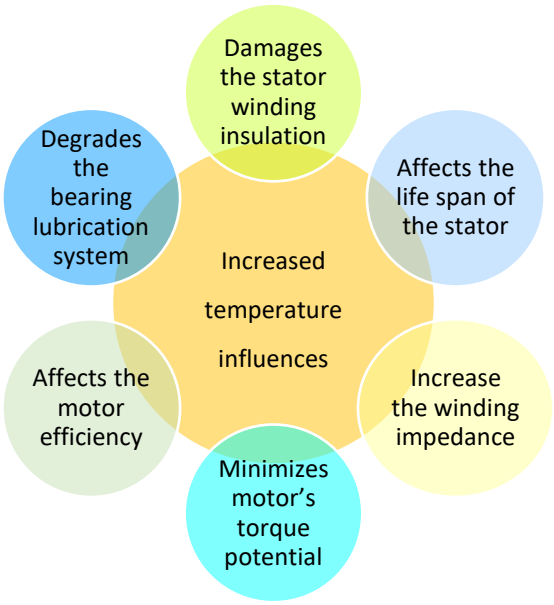

Figure 3. Effects of increasing temperature on the induction motors.

During normal operation, most of the heat generated by the motor's losses is dissipated into the surrounding environment through heat transfer. However, factors such as severe overloading, prolonged starting, or impaired cooling conditions during operation (due to a broken cooling fan or clogged motor case) can affect the cooling capacity of the motor. When the cooling capacity of an IM is compromised, the temperature of the rotor bars and end ring, the stator windings and their insulation may exceed maximum threshold values. Therefore, real-time and accurate monitoring of the temperature of the IM is critical to minimize thermal damage and ensure reliable and safe operation [13]. Correct calculation of temperature rise in electric motors is a critical parameter for the design and operation of the motors. Moreover, temperature rise is also one of the main parameters that limits the rated power of any electric motor. Any uncertainty in predicting the temperature rise at critical points in the motor can result in oversizing the motor, which often involves extra materials, or the motor being rated to produce less power than is needed. Accurate thermal modeling of induction machines is critical to maintaining design integrity, high performance, motor monitoring and protection while reducing costs [14]. Temperature values in electric motors directly affect the performance of the motor. The average temperature is high, especially in businesses that are closed and have high indoor temperatures. High indoor temperatures have a direct negative impact on motor performance. It is known that the life of electric motors decreases with increasing temperature. The increase in the internal temperature of the motor and the increase in the stator winding resistance in direct proportion to the temperature, together with insufficient cooling of the motor housing, have negative effects on the performance of the motor. Therefore, cooling electric motors is important for the operating performance of the motor and energy saving. Cooling in induction motors is generally done by the cooling fins located on the housing, the cooling fins located on the rotor end ring and the fan [7].

Albana et al. made a comparison of six different fin designs and studied their effect on the thermal characteristics of the electric motor. The fins are mounted radially and axially. The six types of fin designs examined are radial fin-round, radial fin-square, radial fin-servo, axial fin-round, axial fin-square, and axial fin-servo. The findings of the study showed that the performance of fins in cooling the electric motor depends on the fin area. It has also been stated that axially mounted fins provide better cooling than radially mounted fins [15]. Appadurai et al. analyzed the effect of cooling fins on the stator frame of an IM using the ANSYS program. They examined the temperature changes in the motor frame by changing the number and height of the fins. From the results, they stated that the efficiency of the fins increased due to the higher length and number of fins, but the volume of the fins also increased, leading to higher motor mass. They showed that optimum efficiency and minimum temperature at the fin tip were obtained by using 44 fins with 15 mm fin length [16]. In their study, Abdullah and Ali investigated the effects of the fins in the stator frame of a 2.2 kW induction motor on the motor temperature. They showed that fin thickness did not have a noticeable difference in motor temperatures, but there was a significant decrease in temperature values with increasing fin depth. They also found that the width between the fins had no effect on the motor temperature, and there was a significant decrease in the stator winding temperature with the increase in the number of fins. They showed that in the absence of any fins in the stator frame, higher temperature values are obtained in the motor compared to the motor with fins [17].

There are many ongoing studies in literature to keep the temperature values of the motors within certain limits. It is seen that these studies are generally in the form of different designs,

modeling/simulation/analysis of the cooling fins located in the stator frame of the motor or the motor fan [18-27].

This study focused on determining the effect of cooling fins on the rotor end ring of three-phase induction motors on motor performance, motor vibration and motor temperature. In the study, experiments were carried out for the performance analysis of healthy motors and motors with shaved rotor cooling fins, and during these experiments, vibration values and thermal images were obtained from various points of the motor. The motivation of the study is to perform both performance and thermal analyses of the faulty motor obtained by shaving the rotor fins compared to the healthy motor and to investigate how these values affect the motor performance.

2. Material and Methods

The motor used in the experiments is a 3-phase, squirrel cage induction motor, source voltage is 400 V, frequency is 50 Hz, motor power is 1100 W, star connected, nominal current value is 2.5 A, 4 poles, stator slot number is 36, shaft diameter is 25 mm, S1 operation, IP55 protection class and F class insulation. The experimental set is given in Figure 4. Autotransformer for voltage regulation, power analyzer for power measurements and torque measurements are obtained by connecting to the experimental set via the load. In addition, a pen type vibration device is used for vibration measurements and a Flir E5 type thermal camera is used for thermal measurements. In addition, a tachometer, digital measuring instruments and a Fucolt brake are used as the load.

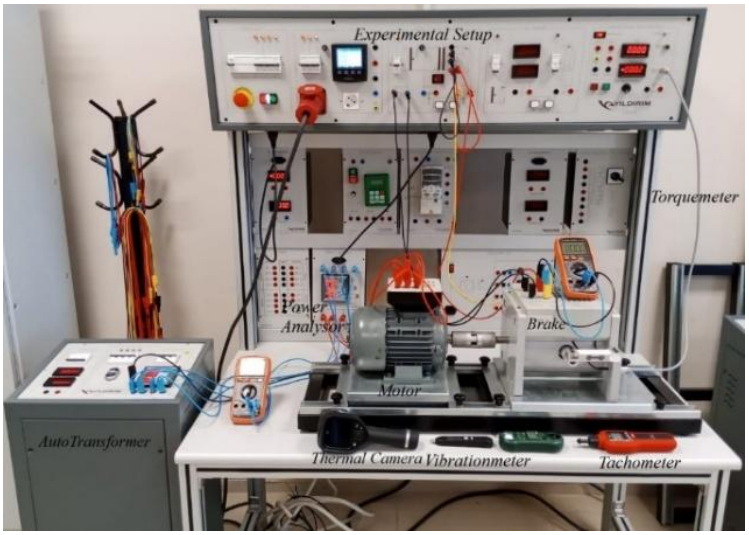

Figure 4. Experimental set-up.

The top and side views of the rotor fins of the healthy motor and the balance screw are given in Figure 5 (a), (b) and (c). The width of the shaved cooling fins is 3 mm, the length is 8.6 mm, and the height is around 12 mm. The diameter of the round cooling fins is 3.2 mm. The total number of shaved fins is 32. All the fins on both sides of the rotor are shaved. As can be seen in Figure 5, the shapes of the fins on the upper and lower parts of the rotor are different from each other and the balance screw is seen. The purpose of this is to ensure the balance in the rotor.

(a) (b) (c)

Figure 5. Rotor fins a) side view b) top view (c) balance screw.

The shaving process of the rotor cooling fins is given in Figure 6 (a). The top and bottom views of the rotor after the shaving process is completed are given in Figure 6 (b) and (c). After the shaving of the fins, the end rings were flattened with sandpaper to remove the roughness.

(a) (b) (c)

Figure 6. (a) Rotor fin shaving process (b) top view (c) bottom view.

After the rotor fins were shaved, the healthy motor and the faulty motor were tested for no-load operation, short circuit operation and loaded operation. The performance of each motor was evaluated using the data obtained from the experiments.

In order to perform performance analysis on induction motors, a single-phase equivalent circuit model is used, and the model is given in Figure 7 [28].

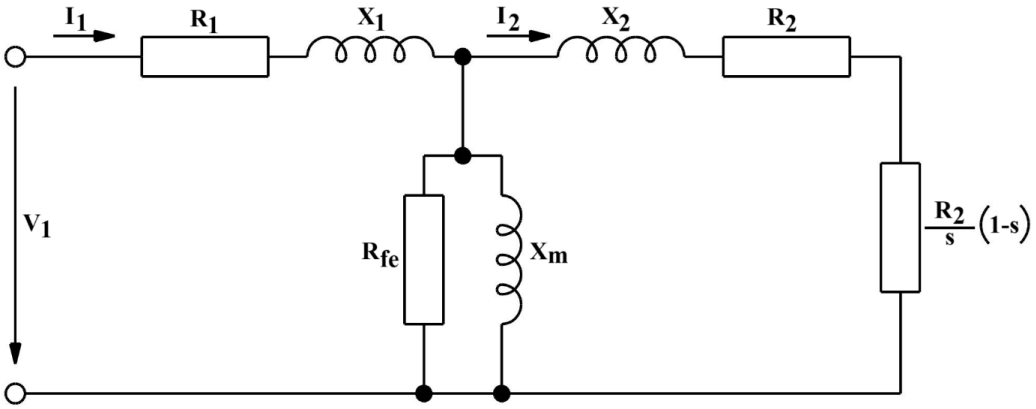

Figure 7. Induction motor single phase equivalent circuit model.

Equivalent circuit parameters of healthy and faulty motors are calculated with the help of the formulas given in Equation 1-5.

The equivalent impedance Zeq value of the induction motor is found with the help of Equation 1. In the equation, Vsc is the short circuit voltage and Isc is the short circuit current.

$$Z_{eq} = \frac{V_{sc}}{I_{sc}} \quad (1)$$

The equivalent resistance (Req) of the motor is calculated as in Equation 2 with the help of copper loss (Pcu) and short circuit current.

$$P_{cu} = 3 \cdot I_{sc}^2 \cdot R_{eq} \quad (2)$$

Equivalent reactance (Xeq) value is calculated as in Equation 3 using equivalent impedance and equivalent resistance.

$$X_{eq} = \sqrt{Z_{eq}^2 - R_{eq}^2} \quad (3)$$

Core resistance (Rfe) and magnetisation reactance (Xm) are found with the help of Equation 4 and Equation 5. In the equations, Vo is the no-load voltage, Pfe is the core losses, Io is the no-load current.

$$R_{fe} = \frac{3 \cdot V_0^2}{P_{fe}} \quad (4)$$

$$X_m = \frac{V_0}{I_0 \cdot Sin_\theta} \quad (5)$$

In induction motors, if the stator resistance is known, the rotor resistance value can be obtained by subtracting the stator resistance from the equivalent resistance value. If the stator resistance value is unknown, the equivalent resistance value is divided into two to obtain both resistances. The same applies to the stator and rotor leakage reactance values, and the equivalent leakage reactance value is divided by two to obtain both leakage reactances.

The efficiency values of the motors are calculated using the output power, core and copper losses as in Equation (6).

$$\eta = \frac{P_{out}}{P_{out}+P_{fe}+P_{cu}} \quad (6)$$

The formula giving the resistance change between the initial and final temperature in the motor is given in Equation (7) [29].

$$R_2 = R_1 \cdot \left(1 + \alpha \cdot (T_2 - T_1)\right) \quad (7)$$

In the equation, R_1 represents the initial resistance value, R_2 represents the final resistance value, α represents the temperature coefficient, and T_1 and T_2 represent the initial and final temperatures, respectively. Here, the temperature coefficient varies depending on the winding material used. Since aluminum is used in the rotor windings, the α value is taken as 0.0038 [30].

In Equation 8, the torque expression obtained depending on the equivalent circuit parameters and the s slip value in induction motors is given. In the expression, f represents the frequency, p represents the number of poles and V_1 represents the fundamental voltage.

$$T = \frac{3 \cdot p}{2 \cdot \pi \cdot f} \cdot \frac{R_2}{s} \cdot \frac{V_1^2}{\left(R_1 + \frac{R_2}{s}\right)^2 + (X_1 + X_2)^2} \quad (8)$$

3. Obtained Results

3.1. Performance analysis

The results and analyses obtained from the experiments conducted on healthy and faulty motors are given below. The experiments were conducted at nominal current and voltage values. The values obtained from the no-load, short-circuit and loaded experiments for both motors are given in Table 1.

Table 1. Experimental data of healthy and faulty motors.

Experiments	Current		Voltage		Power		Speed		Power Factor	
	Healthy M.	Faulty M.	Healthy M.	Faulty M.	Healthy M.	Faulty M.	Healthy M.	Faulty M.	Healthy M.	Faulty M.
No-Load Operation Test	2 A	2.04 A	400 V	400 V	151 W	161 W	1499.8 rpm	1499.8 rpm	0.11	0.12
Short Circuit Test	2.5 A	2.5 A	70 V	70.9 V	211 W	216 W	0	0	0.7	0.72
Load Operation Test	2.5 A	2.5 A	400 V	400 V	1385 W	1368 W	1435 rpm	1432 rpm	0.8	0.79

When Table 1 is examined, it is seen that the current values drawn at no-load are slightly higher for the faulty motor. In terms of core losses, it is seen that the loss value obtained from the faulty motor is 6.62% higher than the healthy motor. In the short circuit test, it is seen that the copper losses are larger for the faulty motor. For both power losses, small increases in the measured current and voltage values and a larger power factor value resulted in an increase in both core and copper losses of the faulty motor compared to the healthy motor.

The obtained equivalent circuit parameters for healthy and faulty motors are given in Table 2. The equivalent circuit parameters are given in ohms.

Table 2. Equivalent circuit parameters of healthy and faulty motors.

Parameters	Healthy M.	Faulty M.	% Difference
Equivalent Impedance (Zeq)	16.165	16.373	1.286
Equivalent Resistance (Req)	11.253	11.520	2.372
Equivalent Reactance (Xeq)	11.605	11.634	0.249
Core Resistance (Rfe)	1059.602	993.788	-6.211
Magnetization Reactance (Xm)	116.284	114.003	-1.961

When the values are examined, it is seen that the equivalent impedance, equivalent resistance and equivalent reactance values for the faulty case increase by a certain amount, and this is because the temperature value of the motor has increased in the faulty case. The fact that the heat cannot be discharged has resulted in an increase in the resistance values. The increase in the resistance has caused the other parameters to increase. There has been a small decrease in the core resistance and magnetization reactance obtained from the no-load values.

Figure 8 shows the torque-speed graph for healthy and faulty motors. The graphs were obtained using the data obtained in Equation 8 and Table 2. When the graph is examined, it is seen that the changes in the equivalent circuit parameters have a greater effect on the motor's maximum torque. At the nominal torque value, it is seen that the torque value of the faulty motor decreases slightly.

It is seen that the temperature values of the faulty motor are higher than the healthy motor, which has a significant effect on the equivalent circuit parameters of the faulty motor. In particular, it is seen that the increase in winding resistance plays a more critical role on the torque-speed characteristics.

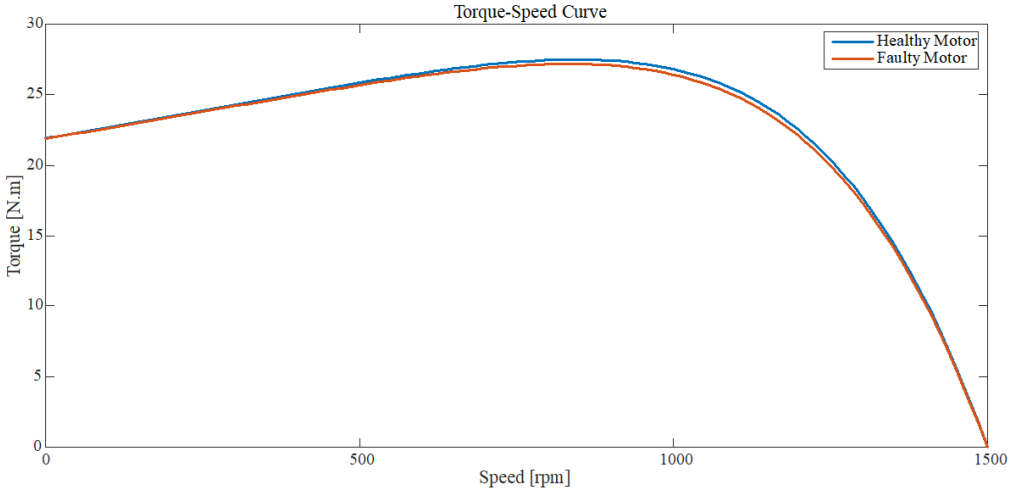

Figure 8. Torque-speed graph of healthy and faulty motors.

The torque values of healthy and faulty motors are given in Table 3.

Table 3. Torque values of healthy and faulty motors.

Parameters	**Healthy Motor**	**Faulty Motor**
Starting Torque [N.m]	21.934	21.898
Maximum Torque [N.m]	27.494	27.182
Nominal Torque [N.m]	7.147	6.983

The efficiency values found by using the core and copper losses obtained for the healthy and faulty motors were obtained as 75.3% for the healthy motor and 74.47% for the faulty motor. It is observed that the efficiency obtained from the faulty motor decreased by 1.01% compared to the healthy motor.

When the performance data obtained from healthy and faulty motors were examined, it was seen that the failure in the rotor fins resulted in an increase in the temperature values on the motor due to the heat in the rotor not being discharged outside, and this negatively affected the motor performance.

3.2. Vibration analysis

Vibrations are an important topic in the field of mechanics and electricity. In the case of electric motors, their presence and magnitude become even more important, since they directly affect the behaviour of the systems in which they are integrated. The sources that cause electric motors to vibrate include electrical imbalance; mechanical imbalance of the rotor and coupling average; consequences of many mechanical problems such as gaps, frictions, bearings and others; consequences of external effects such as poor alignment of some subsystems, such as foundation; resonance, critical speed [31].

Long-term vibration operation of IMs will cause deterioration of motor performance. Vibrations in a motor (medium power) cause structural deformation affecting the stator windings due to the strong electromagnetic force. To meet the industrial requirements, less vibration in motors is mandatory for better efficiency in continuous operation. If the permissible limit is exceeded, it is necessary to identify the cause of increased vibrations [32].

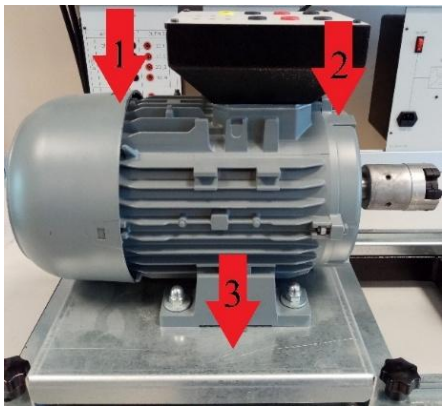

Figure 9. Points where vibration values were measured.

Another analysis performed on the healthy and faulty motor is vibration analysis. As a result of the shaved rotor fins, an imbalance/symmetry disorder will occur in the rotor. The effect of this asymmetrical situation on the vibration values and performance of the motor was investigated. In the literature, it is seen that the measuring devices used to measure vibration in induction motors are connected to different points of the motor

[33, 34, 35]. In this study, vibration values were measured from 3 different points given in Figure 9. The first and second points were measured from the top of the motor, front and rear cover sections. The third measurement point was taken from the table section where the motor feet are located.

The values taken from various points (1-2-3) of the motor using a pen type vibration device for no-load and loaded operation are given in Table 4. Since the motor stops at the time of short circuit, it is not necessary to take any measurement. The vibration values given in Table 4 are in m/s^2.

Table 4. Vibration values of healthy and faulty motors in no-load and loaded operation tests.

Experiments	Point 1		Point 2		Point 3	
	Healthy M.	Faulty M.	Healthy M.	Faulty M.	Healthy M.	Faulty M.
No-Load Operation Test	0.21	0.56	0.48	0.91	2.40	2.45
Load Operation Test	2.63	3.45	1.37	1.68	2.68	3.51

When Table 4 is examined, it is seen that the vibration values for the no-load operation test are lower than 1 m/s^2 at locations 1 and 2. In the loaded operation experiment, it is seen that the values obtained are quite high. The main reason for this situation is that the motor and load shafts are coupled, and this causes an extra vibration to the motor. When the values at point 3 are compared, it is understood that the vibrations in the motor are transferred to the table via the feet. It is also understood that the shaving of the rotor fins for the faulty motor causes an extra vibration in the motor due to the asymmetrical situation. It is seen that all the data obtained for the faulty situation are higher than the healthy motor.

3.3. Thermal analysis

An increase in temperature during operation of an IM can lead to motor failure and a reduction in lifespan. Therefore, the thermal behavior of the IM should be considered as a critical criterion in selecting the motor [36]. In addition, the temperature of electric motors significantly affects the motor parameters. Since the resistance changes of the stator and rotor winding depend on the temperature, the torque-speed characteristics in IM are also affected [37].

Temperature changes in no-load operation, short circuit operation and loaded operation experiments were obtained separately for healthy and faulty motors. The aim here is to show the effect of the fins on the rotor thermally. Figure 10 (a) shows the thermal camera images of the healthy motor during the no-load operation test, (b) the short-circuit operation test, and (c) the loaded operation test. Thermal measurements were made with a Flir E5 handheld thermal camera. Thermal measurements were performed from the motor test set at a distance of 1 meter, which is specified in the camera catalogue. The camera height was adjusted according to the type of experiment.

(a) No-load test (b) Short circuit test (c) Loaded test

Figure 10. Temperature images of the healthy motor.

Figure 11 (a) shows the thermal camera images of the faulty motor during the no-load operation test, (b) the short circuit operation test, and (c) the loaded operation test.

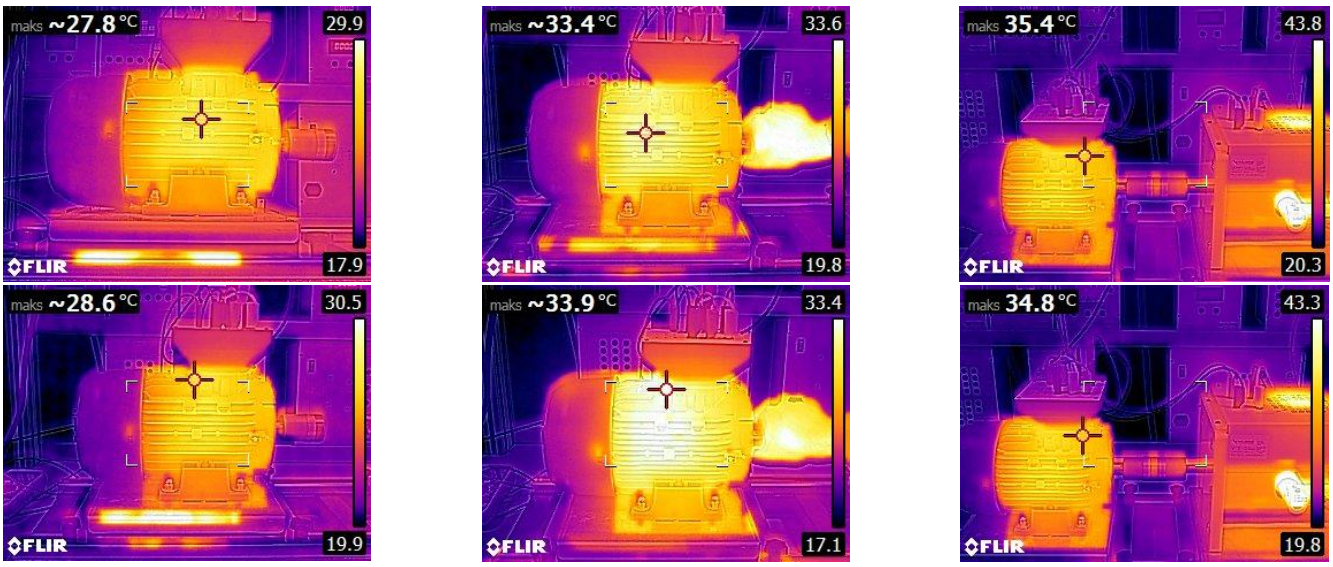

(a) No-load test (b) Short circuit test (c) Loaded test

Figure 11. Temperature images of the faulty motor.

According to the thermal camera images obtained, it was determined that the temperature obtained from the faulty motor was greater than those from the healthy motor in all three studies. It was observed that the highest temperature values for each operating condition were generally obtained from the middle parts of the motors. The values in the temperature graphs for both healthy and faulty motors in Figure 12 and Figure 13 were plotted using the values taken from the hottest point of the motor in the thermal camera measurements. The Flir E5 thermal camera was calibrated to show the hottest point of the motor.

Temperature changes with respect to time obtained from the no-load and loaded operation experiments of both motors are given in Figure 12. Here, measurements were made every 5 minutes, and the experiments were completed in 30 minutes. The laboratory ambient temperature was taken as the initial operating temperature, approximately 22 °C, and this was accepted in all experiments.

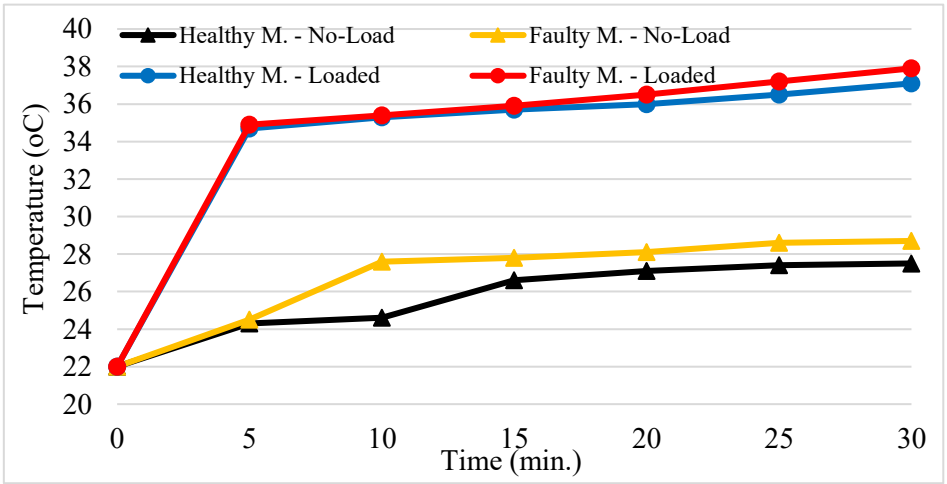

Figure 12. Time-temperature changes for no-load and loaded operating conditions of healthy and faulty motors

When Figure 12 is examined, it is seen that the initial values for both motors in the no-load operation experiment were obtained at room temperature, and the temperature value in the motor increased rapidly as time progressed. It is observed that the temperature progresses at higher values in the faulty case than in the healthy motor in each time period. When the loaded

operation test data is examined, it is seen that although the initial temperature values are almost the same, the faulty motor operates at higher temperatures than the healthy motor as time progresses. In the loaded operation test, it was determined that an increase of 72.27% occurred between the initial and final temperature for the faulty case. When compared with the healthy motor, a 2.15% higher temperature value was obtained for the final temperature value. These values clearly show that the absence of cooling fins on the rotor increases the temperature values in the motor.

The time-temperature changes of both motors during short circuit operation are given in Figure 13.

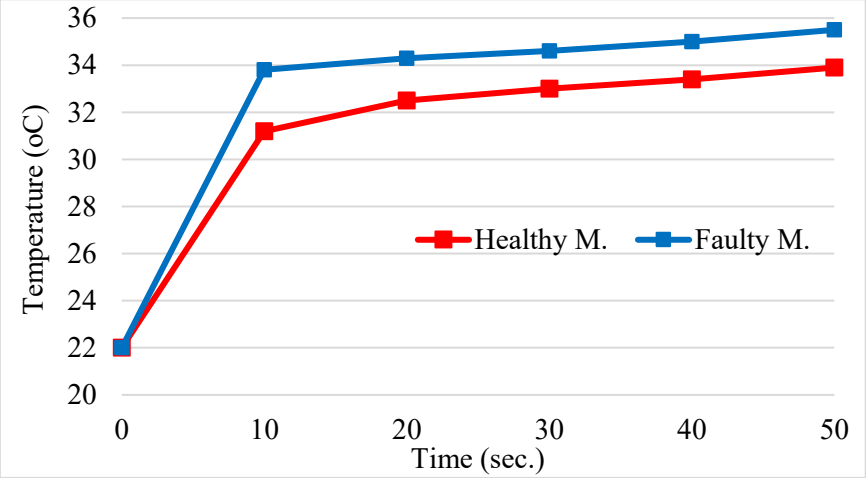

Figure 13. Time-temperature changes for short circuit operation of healthy and faulty motors.

In the short circuit test, the experiment must be completed in a very short time to avoid damage to the motor due to the high current. The experiment was completed in less than 1 minute and it is seen that the temperature values increased rapidly in this short time. It is seen that the temperature value at the last measurement point of the faulty motor increased by 4.72% compared to the healthy motor.

High temperature values in steady state operation will also cause the motor's lost power values to increase. This will result in a decrease in efficiency and negatively affect motor performance.

4. Discussion

Induction motors are widely used in the industry, but an internal or external fault may cause the motor to break down or the process to stop. In the study, the effects of the fault in the rotor cooling fins of a three-phase squirrel cage induction motor on the temperature, vibration and performance of the motor were obtained experimentally.

The shaving of the cooling fins on the rotor end ring has disrupted the rotor balance. In particular, the shaving of the screws used for the rotor balance, as shown in Figure 5c, has caused serious deterioration in the rotor balance, which has caused the motor to operate in a vibrating manner. It is seen that the vibration values obtained from different points are higher for the faulty motor. This shows that the motor operates in an asymmetrical manner.

In another analysis, the temperature parameter, the lack of sufficient cooling in the rotor resulted in higher temperature values in the faulty motor compared to the healthy motor in all three operating conditions. This resulted in an increase in the resistance and reactance values in the faulty motor.

The failure to provide complete cooling in the motor resulted in a negative effect on the performance values of the faulty motor. In fact, differences were obtained in the torque speed graphs of the healthy and faulty motors. An increase in the lost power values occurred, resulting in a 1% decrease in motor efficiency.

5. Conclusion

The aim of this study is to investigate the effects of the failure of the rotor fins, which are located on the rotor end ring of the induction motor and have great importance in cooling the motor, on the thermal, vibration and performance of the IM. Experiments were carried out and analyses were done for both healthy and faulty conditions. According to the thermal data obtained, it was determined that the shaved rotor fins resulted in similar temperature values in the initial measurements during

the no-load operation of the motor, and that the temperature increased more than the healthy motor as time progressed. During the loaded operation tests of the motor, it was observed that the faulty motor operated at higher temperatures than the healthy motor from the beginning of the experiment. Based on the last measured values, it is seen that the temperature value of the faulty motor during loaded operation is 2.15 % higher than that of the healthy motor.

During the short-circuit operation, it was observed that the temperature values increased rapidly due to the high current values, and again the values in the faulty condition were obtained larger than the healthy motor. The temperature value of the faulty motor was 4.72 % higher than that of the healthy motor. This situation also negatively affected the performance of the motor, and a 1% decrease in efficiency occurred. It was observed that a slight decrease in the torque values occurred. The maximum torque value of the faulty motor decreased by 1.13 %.

When the vibration data of the motor were examined, it was seen that the shaving of the rotor fins negatively affected the balance of the motor. It has been determined that the vibration values in the faulty motor are greater than those in the healthy motor, both in no-load and loaded operation. During loaded operation, it was determined that the vibration values, especially at points 1 and 3, were 31% higher.

Acknowledgement

This study was supported by Burdur Mehmet Akif Ersoy University Scientific Research Projects Commission. Project Number: 0691-MP-21.

References

1. Ortiz EDA, Dorantes JJS, Cuellar AYJ, Daviu JAA, Rios RAO. Analysis and detection of broken rotor bars in induction motor under fluctuating load by means of stray flux signals. IEEE Int. Conf. Electr. Mach. 05-08 September 2022, Valencia, Spain, pp. 1816-22. http://dx.doi.org/10.1109/ICEM51905.2022.9910657
2. Abdellah C, Mama C, Abderrahmane M.R.M, Mohammed B. Current park's vector pattern technique for diagnosis of broken rotor bars fault in saturated induction motor. J. Electr. Eng. Technol. 2023;18:2749–2758. https://doi.org/10.1007/s42835-022-01342-6
3. Marek Zastepaa, The statistical-based diagnosis with usage of acoustic sound decomposition and projected LSTM network of induction motors, Eksploatacja i Niezawodnosc–Maintenance and Reliability, 2025;27(3):1-14. http://doi.org/10.17531/ein/205651
4. Basaran M, Fidan M. Induction motor fault classification via entropy and column correlation features of 2D represented vibration data. Eksploatacja i Niezawodnosc–Maintenance and Reliability 2021;23(1):132–142. http://dx.doi.org/10.17531/ein.2021.1.14
5. Costa C, Kashiwagi M, Mathias MH. Rotor failure detection of induction motors by wavelet transform and Fourier transform in non-stationary condition. Case Stud. Mech. Syst. Signal Process. 2015;1:15–26. http://dx.doi.org/10.1016/j.csmssp.2015.05.001
6. Sharma A, Mathew L, Chatterji S. Analysis of broken rotor bar fault diagnosis for induction motor. Int. Conf. Innovations Control Commun. Inf. Syst. 12-13 August 2017, Greater Noida, India pp. 1-5. http://dx.doi.org/10.1109/ICICCIS.2017.8660808
7. Çakmak YE, Yetgin AG. Investigation of the effects of frame fin failure on motor performance of a three phase squirrel cage induction motor. 4. Baskent Int. Conf. Multi. Stud. 4-6 August 2023, Ankara Türkiye, pp. 297-304.
8. Dehina W, Boumehraz M, Kratz F. Detectability of rotor failure for induction motors through stator current based on advanced signal processing approaches. Int. J. Dyn. Control 2021;9:1381–95. https://doi.org/10.1007/s40435-021-00765-9
9. Halder S, Bhat S, Zychma D, Sowa P. Broken rotor bar fault diagnosis techniques based on motor current signature analysis for induction motor-A review. Energies 2022;15:1-20. https://doi.org/10.3390/en15228569
10. Prasad KVSR, Singh V. Fault diagnosis of induction machine for rotor cage damage using mcsa for industrial application. Electr. Power Compon. Syst. 2024;0:1-13. http://dx.doi.org/10.1080/15325008.2024.2350697
11. Bahgat BH, Elhay EA, Elkholy MM. Advanced fault detection technique of three phase induction motor: comprehensive review. Discover Electron. 2024;1(9):1-25. https://doi.org/10.1007/s44291-024-00012-3
12. Badran O, Sarhan H, Alomour B. Thermal performance analysis of induction motor. Int. J. Heat Technol. 2012;30(1):75-88. https://doi.org/10.18280/ijht.300112
13. Konda YR, Ponnaganti VK, Reddy PVS, Singh RR, Mercorelli P, Gundabattini E, Solomon DG. Thermal analysis and cooling strategies

of high-efficiency three-phase squirrel-cage induction motors-A review. Comput. 2024;12:1-21. https://doi.org/10.3390/computation12010006

14. Xie Y, Wang Y. 3D temperature field analysis of the induction motors with broken bar fault. Appl. Therm. Eng. 2014;66:25-34. http://dx.doi.org/10.1016/j.applthermaleng.2014.02.008
15. Albana MH, Guntur HL, Putra ABK. The effect of fins design on the thermal characteristics of electric motors for electric vehicles. IEEE Int. Conf. Adv. Mechatron. Intell. Manuf. Ind. Autom. 14-15 November 2023, Surabaya, Indonesia, pp. 1-6. https://doi.org/10.1109/ICAMIMIA60881.2023.10427619
16. Appadurai M, Raj EFI, Venkadeshwaran K. Finite element design and thermal analysis of an induction motor used for a hydraulic pumping system. Mater. Today Proc. 2021;45:7100-06. https://doi.org/10.1016/j.matpr.2021.01.944
17. Abdullah AT, Ali AM. Thermal analysis of a three-phase induction motor with frame design considerations. IOP Conf. Ser.: Mater. Sci. Eng. 2019;518:1-10. https://doi.org/10.1088/1757-899X/518/4/042010
18. Ulbrich S, Kopte J, Proske J. Cooling fin optimization on a tefc electrical machine housing using a 2-D conjugate heat transfer model. IEEE Trans. Ind. Electron. 2018;65(2):1711-18. https://doi.org/10.1109/TIE.2017.2748051
19. Madhavan S, Devdatta PBR, Gundabattini E, Mystkowski A. Thermal analysis and heat management strategies for an induction motor, a review. Energies 2022;15:1-20. https://doi.org/10.3390/en15218127
20. Roffi M, Ferreira FJTE, Almeida ATD. Comparison of different cooling fan designs for electric motors. IEEE Int. Electr. Mach. Drives Conf. 21-24 May 2017, Miami, FL, USA, pp. 1-7. https://doi.org/10.1109/IEMDC.2017.8002270
21. Ghahfarokhi PS, Kallaste A, Podgornovs A, Belahcen A, Vaimann T, Asad B. Determination of heat transfer coefficient of finned housing of a TEFC variable speed motor. Electr. Eng. 2021;103:1009-17. https://doi.org/10.1007/s00202-020-01132-1
22. Bhambere MB, Chaudhari SS. Numerical analysis of heat transfer from perforated fins of an induction motor housing. IOP Conf. Ser.: Mater. Sci. Eng. 2022;1259:1-7. https://doi.org/10.1088/1757-899X/1259/1/012011
23. Koa MJ, Leea SH, Parka SS. IE4-class 2.2-kW induction motor design and performance evaluation. J. Korean Soc. Manuf. Technol. Eng. 2021;30(5):345-51. https://doi.org/10.7735/ksmte.2021.30.5.345
24. Goh S, Fawzal AS, Gyftakis KN, Cardoso AJM. Impact of the fan design and rotational direction on the thermal characteristics of induction motors. IEEE XIII Int. Conf. Electr. Mach. 03-06 September 2018, Alexandroupoli, Greece, pp. 1-7. https://dx.doi.org/10.1109/ICELMACH.2018.8506974
25. Chen L, Liu XJ, Yang AL, Dai R. Flow performance of highly loaded axial fan with bowed rotor blades. IOP Conf. Series: Mater. Sci. Eng. 2013;52:1-8. https://dx.doi.org/10.1088/1757-899X/52/4/042005
26. Kim C, Lee KS, Yook SJ. Effect of air-gap fans on cooling of windings in a large-capacity, high-speed induction motor. Appl. Therm. Eng. 2016;100:658–67. http://dx.doi.org/10.1016/j.applthermaleng.2016.02.077
27. Özyildiz T, Lüle SŞ. The fan design optimization for totally enclosed type induction motor with experimentally verified cfd-based moga simulations. Arabian J. Sci. Eng. 2024;49:15597-610. https://doi.org/10.1007/s13369-024-09134-y
28. Torrent M, Blanque B. Influence of equivalent circuit resistances on operating parameters on three-phase induction motors with powers up to 50 kW. Energies 2021;14:1-22. https://doi.org/10.3390/en14217130
29. Marangoni TA, Guralnik B, Borup KA, Hansen O, Petersen DH. Determination of the temperature coefficient of resistance from micro four-point probe measurements. J. Appl. Phys. 2021;129:1-9. https://doi.org/10.1063/5.0046591
30. Bird J. Electrical circuit theory and technology, Chapter 3: resistance variation, (Second Edition), 23-29, Elsevier Science, Great Britain, 2003.
31. Ioan P, Arpad B. A Study on the vibrations of the induction motors having squirrel cage rotor. Eng. Today 2023;2(1):23-30. https://doi.org/10.5937/engtoday2300002P
32. Prasad KVSR, Rao KD, Alsaif F. Induction motor structure design to reduce vibrations with numerical (fea) and experimental (va) techniques. IEEE Access 2024;12:40894-904. https://doi.org/10.1109/ACCESS.2024.3374785
33. Gabriela R, Mihai R. System for Monitoring and Analysis of Vibrat ions at Electric Motors. Analele Universitatii Eftimie Murgu Resita 2014;21(3):97-104.
34. Dipesh BP, Mahadev GU, Shraddha M, Dhanshri AN. Condition monitoring of induction motor-vibration analysis technique. Int. J. Eng.

Sci. Technol. 2022;14(3):38-46. http://dx.doi.org/10.4314/ijest.v14i3.5S

35. Pedro VJR. Current-, force-, and vibration-based techniques for induction motor condition monitoring. Doctoral Dissertation, Helsinki University of Technology, Department of Electrical and Communications Engineering, 2007;1-86.
36. Cabral P, Adouni A. Induction motor thermal analysis based on lumped parameter thermal network. Int. Congr. Eng.-Eng. Evol. 2020;451–64. https://doi.org/10.18502/keg.v5i6.7061
37. Sudha B, Vadde A, Manickavasagam K, Kadambi GR. Characterization of temperature and productive torque for 160l frame squirrel cage induction motor. J. Eng. Res. 2021;Special Issue:35-46. https://doi.org/10.36909/jer.EMSME.13853